J. Iron Steel Res. Int. (2023) 30:1356–1366
https://doi.org/10.1007/s42243-023-00985-7

ORIGINAL PAPER

Effect of quaternary basicity on reduction behavior of iron-bearing dust pellets

Tao Yang[1] · Jing-shu An[1] · Xing-wang Li[1] · Shuang Liu[1] · Xu Gao[1] · Lei Ma[1] · Jie Lei[1] · Hong-ming Long[1,2]

Received: 15 December 2022 / Revised: 28 February 2023 / Accepted: 17 March 2023 / Published online: 23 May 2023

Abstract
The treatment of iron-bearing dusts and sludges by the rotary hearth furnace process has the advantage of sufficient utilization of valuable metals and a high impurity removal rate, but the lower strength of the metallized product needs to be addressed. The effects of quaternary basicity R_4 ($w(CaO + MgO)/w(SiO_2 + Al_2O_3)$) on the reduction behavior and physical and chemical properties of metallized pellets, including phase composition, compressive strength, microstructure and soft melting area, were investigated with FactSage thermodynamic software and experiments. The strength of metallized pellets depended on the gangue composition, such as CaO, MgO, Al_2O_3 and SiO_2, due to the altered chemical composition, physical phase composition, microscopic morphology and stability of the slag phase. The reduction of carbon-bearing pellets was significantly promoted by suitable basicity. The lower basicity ($R_4 < 1.4$) facilitated the formation of low melting point iron-containing compounds from SiO_2 and Al_2O_3 with FeO, resulting in increased liquid phase generation, but lower metallization rate, due to the hindered precipitation and growth of iron grains. Interestingly, the higher basicity ($R_4 > 1.8$) also increased the amount of liquid phase and improved the strength of the pellets, due to the granular iron crystals bonded into sheets. Notably, the main component of the liquid phase in high-basicity conditions was calcium ferrite. Although the additional amount of liquid phase was beneficial to the strength of the metallized pellets, calcium disilicate was formed at $R_4 = 1.6$, resulting in a reduction in the compressive strength of the pellets to 1521.9 N/pellet.

Keywords Metallurgical solid waste · Iron-bearing dust · Iron-bearing sludge · Rotary hearth furnace · Quaternary basicity · Metallized pellet · High-temperature performance

1 Introduction

Solid wastes (metallurgical dusts, sludges, etc.) generated by the steel production process have the characteristics of a wide range of sources, large production volume and complex composition [1–5], causing difficulties in the disposal. In general, metallurgical dusts and sludges contain valuable elements and compounds, such as Fe, Zn, Pb and C [6–8], providing a high recycling value. Most of the metallurgical solid wastes are discarded or landfilled, resulting in the waste of valuable elements and environmental pollution.

Research on the efficient recovery and purification of valuable elements from metallurgical dusts and sludges has attracted widespread attention. The processes for recycling were divided into three main categories [9]: pyrometallurgical process, wet process and physical process. The wet treatment process is initiated by selecting appropriate leaching agents to leach the valuable elements such as Zn, Pb, In and Bi from the metallurgical dusts and sludges [10–13]. Sulfuric acid, hydrochloric acid and caustic soda are commonly employed as the leaching agents. Numerous experiments have established that the wet treatment process has relatively superior leaching selectivity and a high degree of integrated recovery of valuable metals. However, serious secondary pollution, high cost and low yield have limited commercialization. Physical methods [14–16]

✉ Hong-ming Long
yaflhm@126.com

[1] School of Metallurgical Engineering, Anhui University of Technology, Ma'anshan 243032, Anhui, China

[2] Key Laboratory of Metallurgical Emission Reduction & Resources Recycling (Anhui University of Technology), Ministry of Education, Ma'anshan 243002, Anhui, China

include magnetic separation, mechanical separation, hydrocyclone dezincification, flotation and combinations of these methods. Physical methods allow the separation and recovery of valuable elements directly from metallurgical dusts and sludges, but require suitable physical properties. The physical treatment process is simple, low investment and no secondary pollution [17–21], but has high-power consumption and low removal efficiency of valuable elements. Therefore, the physical method is gradually replaced by the coal-based direct reduction process. Pyrometallurgical processes reduce metal oxides at high temperature by carbothermal reduction reactions. In addition, the valuable elements (e.g., Zn and Pb) will be volatilized and captured at high temperature. The rotary hearth furnace process, a typical current thermal treatment process for iron-bearing dusts and sludges, provides a novel avenue for the production of metallized raw materials and the utilization of iron-bearing secondary resources. Numerous literatures reported that the rotary hearth furnace process exhibits the advantages of a high impurity removal rate and excellent product metallization [17, 22–25]. Thus far, the rotary hearth furnace process has become one of the future development frameworks for iron-bearing dusts and sludges treatment technology in steel companies. Notably, industrial practice indicated that metallized pellets are prone to breakage and pulverization during reduction and cooling in rotary hearth furnaces [26–29]. The fine dusts blocked the gaps between the pellets, which deteriorated the reduction kinetics of metallized pellets inside the rotary hearth furnace, resulting in a lower metallization rate and removal rate of harmful elements such as zinc of the pellets and leading to a significant decrease in yield and strength, which cannot meet the requirements of the subsequent steelmaking or ironmaking process. Therefore, the reduction mechanism [30–32], kinetics of the reduction reaction [33–38] and factors affecting the reduction intensity [39, 40] of metallized microspheres have been intensively investigated by scholars. It was suggested that the strength of iron ore pellets was related to the gangue composition, as the gangue had a significant effect on the formation, composition, microscopic morphology and stability of the bonded phase at high temperature [41–43]. Fan et al. [44] and Wu et al. [45] found that the addition of a moderate amount of CaO leads to the formation of FeO by substitution reactions of difficult-to-reduce iron-containing compounds such as $2FeO{\cdot}SiO_2$ and $2FeO{\cdot}Al_2O_3$. The reduction efficiency of carbon-bearing pellets was improved. However, the increased melting point of the reduced system enhanced the difficulty of iron diffusion and migration in the gangue phase, affecting the growth of metallic iron particles. Zhang et al. [46] investigated the effect of MgO addition on the properties of carbon-bearing pellets. The raw pellet properties were significantly improved with the addition of MgO, but the compressive strength of the roasted pellets decreased, due to the increase in the melting temperature of the slag phase generation with the addition of MgO, which led to the decrease in the amount of liquid phase.

A major current focus in extensive studies is the effect of single gangue composition (such as CaO, MgO, Al_2O_3 and SiO_2) on the reduction behavior of carbon-bearing pellets. However, the synergistic effects among different gangue compositions have not been clearly explored. In particular, the relationship between the quaternary basicity of carbon-bearing pellets prepared from metallurgical dusts and sludges and their physicochemical properties such as strength has not been clearly clarified. For this gap, the influence of quaternary basicity R_4 on the composition and content of the bonding phase, the strength of the carbon-bearing pellets and the changes in the melt properties at high temperature were investigated. Theoretical guidance and technical support were provided for the process of metallurgical dusts and sludges treatment in the rotary hearth furnace.

2 Experimental

2.1 Materials

In this study, the raw materials were collected from the rotary hearth furnace of a Chinese steel company. The main iron-bearing raw materials included blast furnace (BF) bag dust after washing and dechlorination, oxygen converter gas recovery (OG) mixed dust and rotary hearth furnace (RHF) dust. The OG mixed dust was generated from the cleaning of the primary exhaust gas system of steelmaking processes such as basic oxygen furnace (BOF) and electric arc furnace (EAF). The RHF dust includes fly ash produced during the transportation of raw materials and the new-formed dusts due to pellets breakage. Table 1 shows the chemical composition of the iron-bearing dusts and sludges, as determined by X-ray fluorescence (XRF, ARLAdvant'X Intellipower 3600) analysis. As shown in Table 1, the carbon content of BF bag dust was 33.57 wt.%, recognized as the main source of reducing agent in carbon-bearing pellets. The OG mixed dust was a high-basicity iron-bearing dust and sludge, due to the TFe content of 57.51 wt.% and R_4 of 4.72. The binder for pellet forming was a composite binder of bentonite and organic starch. R_4 was adjusted by adding SiO_2 and $Ca(OH)_2$ (analytical reagent).

Table 1 Chemical composition of iron-bearing dusts and sludges

Sample	Chemical composition/wt.%											R_4
	TFe	FeO	C	Zn	SiO_2	Al_2O_3	CaO	MgO	K_2O	Na_2O	PbO	
BF bag dust	24.59	5.62	33.57	3.75	7.14	4.43	3.26	2.32	0.53	0.59	0.91	0.48
OG mixed dust	57.51	53.47	2.28	1.47	2.54	0.36	11.52	2.19	0.18	0.27	0.18	4.72
RHF dust	44.7	46.61	15.25	2.18	6.36	2.28	8.11	1.97	0.34	0.38	0.41	1.17

R_4=w(CaO+MgO)/w(SiO_2+Al_2O_3)

2.2 Methods

The mixing ratios of iron-bearing dusts and sludges with SiO_2 and $Ca(OH)_2$ in each scheme are given in Table 2. The addition ratios of SiO_2, $Ca(OH)_2$ and binder were the proportion of the substance to the total mass of the powder mixture. The ratio of carbon to oxygen ($C/O_{reducible}$) for the reduction test was 0.9 ($C/O_{reducible}$ was obtained from the actual production data of the rotary hearth furnace process in a Chinese steel company). The patterns of high-temperature strength, microstructure, metallization rate and dezincification rate of carbon-bearing pellets were examined with different R_4 (1.0, 1.2, 1.4, 1.6, 1.8, 2.0 and 2.2). The test process included raw material preparation, green pellets production, drying, roasting and comprehensive performance testing. The iron-bearing dusts and sludges and binder were fully mixed and supplemented with water to 14% according to the batching scheme in Table 2. The carbon-bearing pellets were prepared using a hydraulic twin-roller machine with roller linear pressure of 2.35×10^4 N cm^{-1} and roller speed of 5.0 r min^{-1}, and the pressed carbon-bearing pellets were ellipsoidal in shape, with length of 15 mm, width of 25 mm and thickness of 32 mm. The green pellets were dried in a blast drying oven at 110 °C for 8 h, and the qualified dry pellets were selected and loaded into the crucible. The reducing experiments were carried out in a horizontal electric heating furnace in a nitrogen atmosphere, as shown in Fig. 1. The reduction temperature and reduction time were 1275 °C and 25 min, respectively. In order to prevent the reduced metallized pellets from reoxidation, nitrogen was introduced into the furnace to decrease the oxygen content, and the crucible was removed and then covered with a nitrogen-filled stainless steel protective cover to lower the temperature down below 200 °C.

The compressive strength of metallized pellets was determined on a pellets strength tester. The strength test was averaged for 10 times under the same conditions. The phase evolution of metallized pellets with different alkalinities was studied using an X-ray powder diffractometer (Bruker D8 Advance, nickel-filtered Cu Kα radiation, 40 kV, λ = 0.15418 nm). The diffractograms were measured in the 2θ range of 10°–90° with a scanning rate of 10 (°)/min. An automatic polishing machine was used to polish the metallized pellets. Polished samples were used to observe the microstructure evolution and phase composition of metallized pellets under a metalloscope (Carl Zeiss Axio Scope.A1). The high-temperature physical property measuring instrument can observe the morphological changes of the melt during the heating process in real-time. The high-temperature physical properties of the melt were expressed in terms of the change in melt area. Figure 2 shows the high-temperature physical property measuring instrument. The furnace was heated up to 1275 °C, and

Table 2 Raw material ratio of carbon-bearing pellets

Scheme	Raw material ratio/%						$C/O_{reducible}$	R_4
	BF bag dust	OG mixed dust	RHF dust	SiO_2	$Ca(OH)_2$	Binder		
J1	25.1	65.9	9.0	–	1.32	3.0	0.9	2.2
J2	25.1	65.9	9.0	–	–	3.0	0.9	2.0
J3	25.1	65.9	9.0	0.71	–	3.0	0.9	1.8
J4	25.1	65.9	9.0	1.50	–	3.0	0.9	1.6
J5	25.1	65.9	9.0	2.51	–	3.0	0.9	1.4
J6	25.1	65.9	9.0	3.86	–	3.0	0.9	1.2
J7	25.1	65.9	9.0	5.66	–	3.0	0.9	1.0

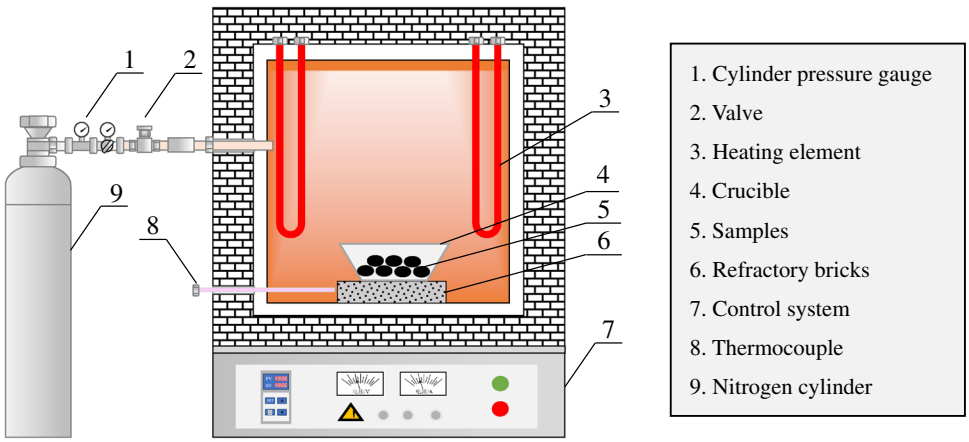

Fig. 1 High-temperature reduction test setup for carbon-bearing pellets

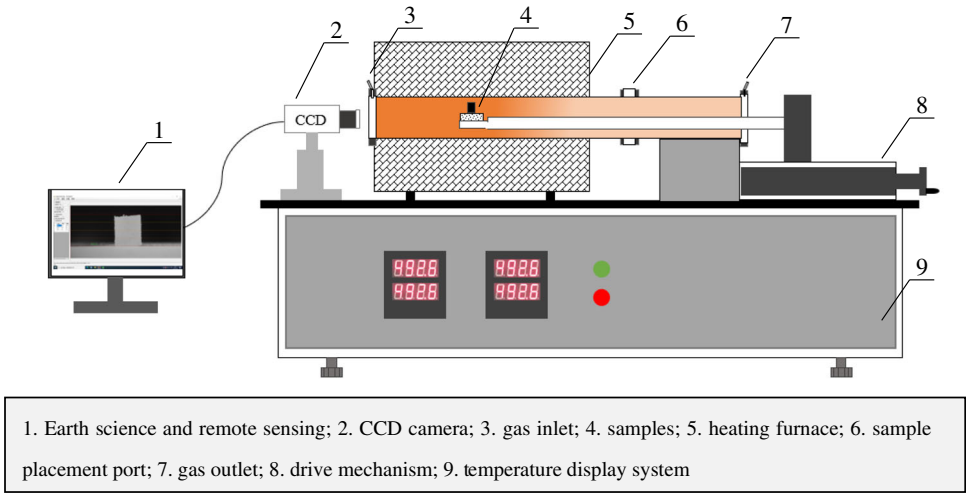

Fig. 2 High-temperature physical property measuring instrument

nitrogen gas was introduced into the chamber. The samples with different alkalinities were sent to the constant temperature region by the drive mechanism, and the morphological changes of the samples during the heating process were started to be recorded.

3 Results and discussion

3.1 Theoretical investigation of bonded phase generation behavior

In order to avoid the degradation of the phase due to unreasonable composition, thermodynamic calculations by Equilib module in FactSage 7.1 were carried out. The equilibrium phase composition and liquid phase components of the reduced system under different R_4 conditions were derived. The theoretical calculations guided the design of the experimental schemes and the validation of the results. The theoretical calculation temperature was 1275 °C, and the pressure was 101.325 kPa. The theoretical initial composition of the raw materials under different R_4 conditions is shown in Table 3, as calculated by the material balance from the batching scheme in Table 2.

Figure 3 shows the ternary contour phase diagram of the FeO–SiO_2–CaO system with different $w(Al_2O_3 + MgO)$ contents at 1275 °C. The dashed lines in the diagram represent the same basicity. The different colors represent the high and low liquid phase generation. The amount of liquid phase gradually decreases when the $w(Al_2O_3 + MgO)$ content was increased from 11 to 19 wt.%. This indicates that the increase in $w(Al_2O_3 + MgO)$ was detrimental to the generation of the liquid phase. At the same $w(Al_2O_3 + MgO)$ content, the FeO content had a significant effect on the experimental results. At higher FeO content, the amount of liquid phase generation decreases with the increase in R_4. At lower FeO content, the amount of liquid phase generation showed a

Table 3 Theoretical calculation of initial composition of raw materials under different R_4 conditions

R_4	Initial composition/wt.%								
	TFe	Fe_2O_3	FeO	C	ZnO	SiO_2	Al_2O_3	CaO	MgO
2.20	47.64	23.11	40.45	11.19	2.60	4.00	1.54	10.00	2.18
2.10	47.90	23.23	40.68	11.25	2.61	4.02	1.55	9.50	2.19
2.00	48.10	23.33	40.84	11.30	2.62	4.04	1.56	9.14	2.20
1.90	47.92	23.24	40.69	11.26	2.61	4.40	1.55	9.11	2.19
1.80	47.77	23.17	40.57	11.22	2.61	4.68	1.54	9.08	2.19
1.70	47.58	23.08	40.41	11.18	2.60	5.06	1.54	9.04	2.18
1.60	47.39	22.98	40.24	11.13	2.59	5.46	1.53	9.01	2.17
1.50	47.17	22.88	40.05	11.08	2.57	5.89	1.53	8.96	2.16
1.40	46.92	22.76	39.84	11.02	2.56	6.39	1.52	8.92	2.15
1.30	46.64	22.62	39.60	10.96	2.54	6.95	1.51	8.86	2.14
1.20	46.31	22.46	39.33	10.88	2.53	7.60	1.50	8.80	2.12
1.10	45.93	22.28	39.00	10.79	2.51	8.36	1.49	8.73	2.10
1.00	45.48	22.06	38.62	10.69	2.48	9.25	1.47	8.64	2.08
0.90	44.95	21.80	38.17	10.56	2.45	10.32	1.45	8.54	2.06
0.80	44.30	21.48	37.62	10.41	2.42	11.62	1.43	8.42	2.03
0.70	43.48	21.09	36.92	10.21	2.37	13.24	1.41	8.26	1.99
0.60	42.45	20.59	36.05	9.97	2.32	15.31	1.37	8.07	1.94

trend of decreasing first and then slightly increasing with the increase in R_4. At the same basicity and $w(Al_2O_3 + MgO)$ content, the amount of liquid phase generation increased significantly with increasing the FeO content. In general, the volume of the liquid phase in the system reaches almost 100% at R_4 of around 0.8. Less liquid phase was generated at R_4 of 1.2–1.8 and low FeO content region (less than 10 wt.%).

Figure 4a shows the equilibrium phase composition of the carbon-bearing pellets with different R_4 at 1275 °C. It can be seen that as the R_4 increases from 0.6 to 2.2, the high melting point slag phases such as melilite (melting point: 1450 °C), merwinite (melting point: 1550 °C), bredigite (melting point: 1372 °C) and calcium disilicate (melting point: 2130 °C) were generated sequentially, making it difficult to obtain more liquid phases by heating. The composition and viscosity of the liquid phase are given in Fig. 4b and c. The content of FeO in the liquid phase remained stable with the increase in basicity, while the contents of SiO_2 and MgO decreased, and the contents of CaO and Al_2O_3 increased. Meanwhile, the increase in basicity leads to a decrease in the viscosity of the liquid phase from 1.547 Pa s (R_4 = 0.6) to 0.220 Pa s (R_4 = 2.2). The liquid phase fluidity was improved. The elemental diffusion and the aggregation and growth of iron particles were promoted, thus improving the solidification properties of the carbon-bearing pellets.

3.2 Effect of R_4 on reduction performance of metallized pellets

Figure 5 shows the morphology of the metallized pellets after roasting from various experimental schemes. The liquid phase was produced in large quantities at R_4 of 1.0 and gradually filled the voids inside the pellets. The excessive liquid phase overflowed to the surface of the pellets. The liquid phase yield and pellets volume gradually decreased with the gradual increase in R_4, and even if there is more fluid, the liquid phase cannot overflow from the pellets because it is less, so that the liquid phase overflowing from the surface gradually disappeared. It should be pointed out that when the R_4 was 1.4–1.8, numerous cracks appeared on the surface of the pellets, and the size of the pellets increased as well, indicating that the pellets underwent malignant expansion. As R_4 continued to increase, the particle surface cracking decreased. Figure 6 shows the influence of the R_4 addition on the compressive strength of the metallized pellets after roasting. As can be seen, the variation rule of compressive strength and the theoretical liquid phase generation were consistent at R_4 of 1.0–2.2. The compressive strength of metallized pellets showed a trend of first decreasing and then increasing when the R_4 was increased from 1.0 to 2.2. The compressive strength reached a minimum value at R_4 of 1.6, decreasing

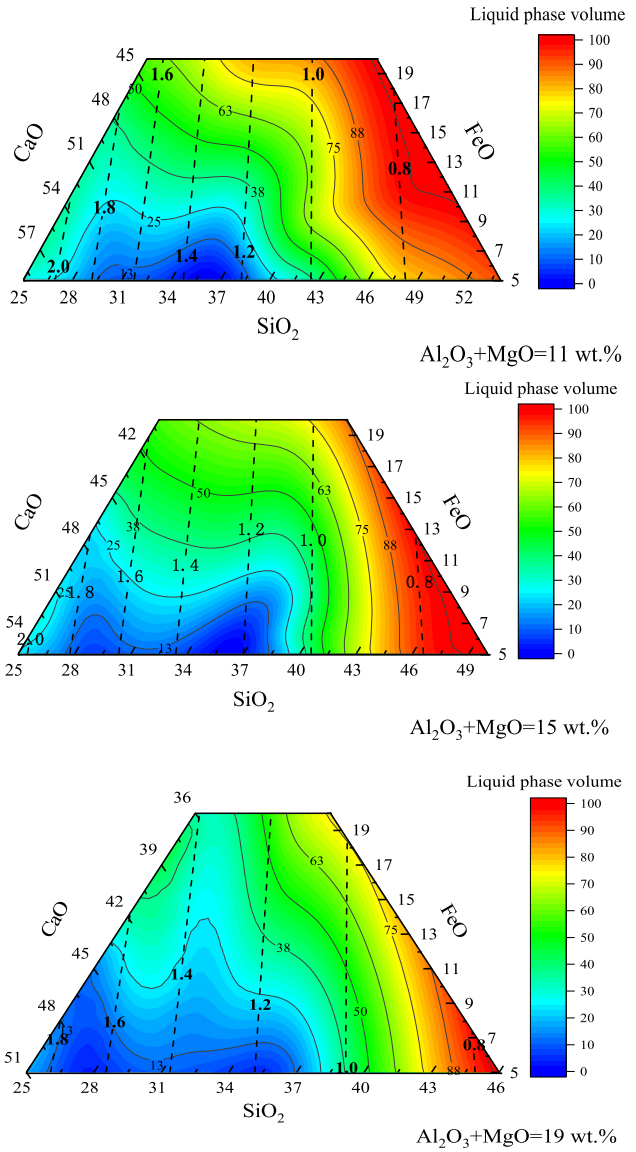

Fig. 3 Ternary contour phase diagram of FeO–SiO_2–CaO system with different $w(Al_2O_3 + MgO)$ contents

from 2678.4 to 1521.9 N/pellet and increasing to 2099.6 N/pellet when the R_4 was increased to 2.2.

The metallization rate and dezincification rate of metallized pellets from various experimental schemes are shown in Fig. 7. Admittedly, the metallization rate exhibited a trend of increasing and subsequently decreasing with the increase in R_4, in contrast with the trend of compressive strength. At R_4 of 1.6 and 1.8, the metallization rate reached larger values of 98.65% and 98.64%, respectively. When the R_4 was higher than 1.4, the dezincification rate was higher than 99%.

To clarify the effect of R_4 on the compressive strength of metallized pellets, the mineral phases of the reduction products were analyzed. Figure 8 shows the X-ray diffraction (XRD) patterns of the metallized pellets after

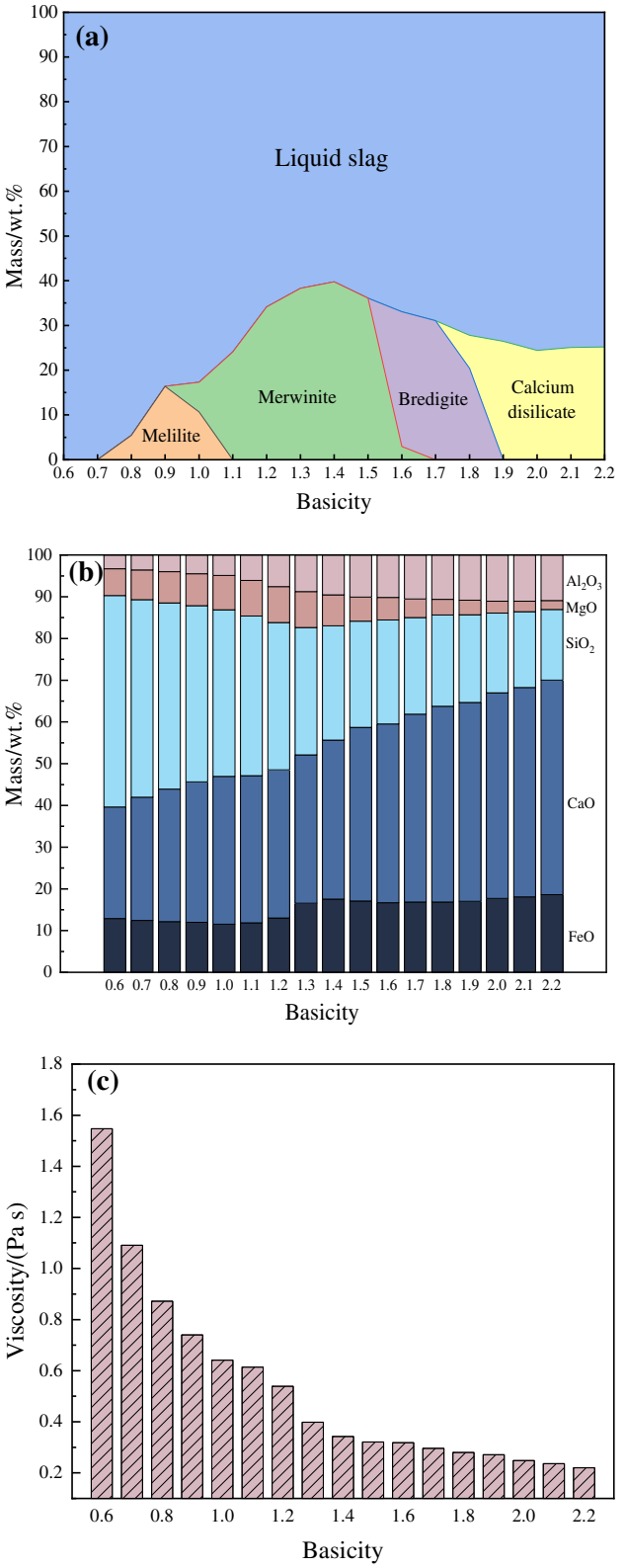

Fig. 4 Influence of R_4 increase on bonded phase generation behavior. **a** Equilibrium phase composition; **b** composition of liquid phase and **c** viscosity of liquid phase

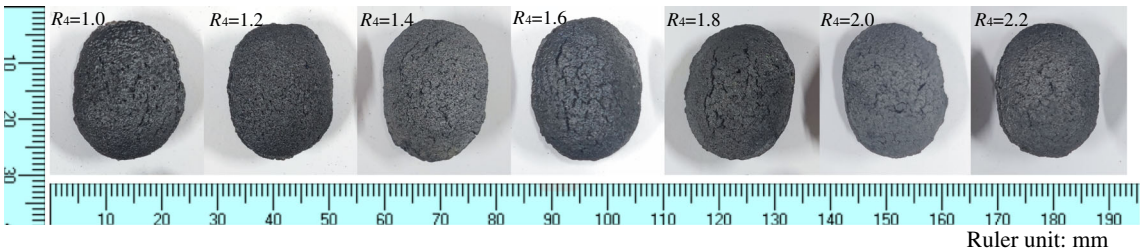

Fig. 5 Influence of R_4 on morphology of metallized pellets

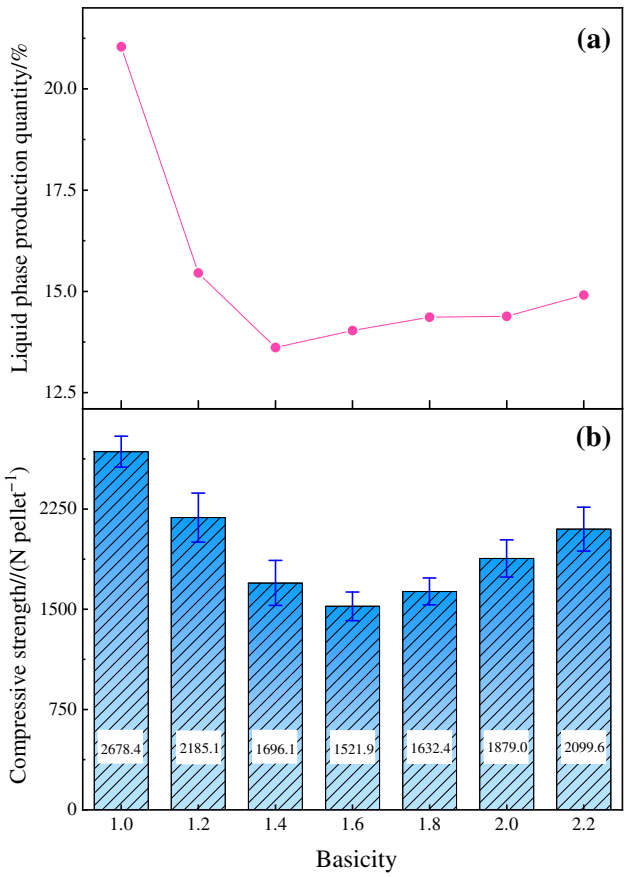

Fig. 6 Influence of R_4 on performance of metallized pellets. **a** Theoretical liquid phase production quantity; **b** compressive strength

roasting from various experimental schemes. The XRD peaks of metallized pellets were mainly of metallic iron, and the peaks of other forms of iron oxides were lower. This result indicated that the iron oxides in the metallized pellets have been almost completely reduced to metallic iron. The peak intensity of metallic iron showed a trend of first increasing and then decreasing with the increase in basicity, which is consistent with the variation rule of the metallization rate of the metallized pellets. The bonding phase inside the metallized pellets primarily existed as silicate when R_4 was less than 1.4. The voids inside the pellets due to binder volatilization, carbon consumption

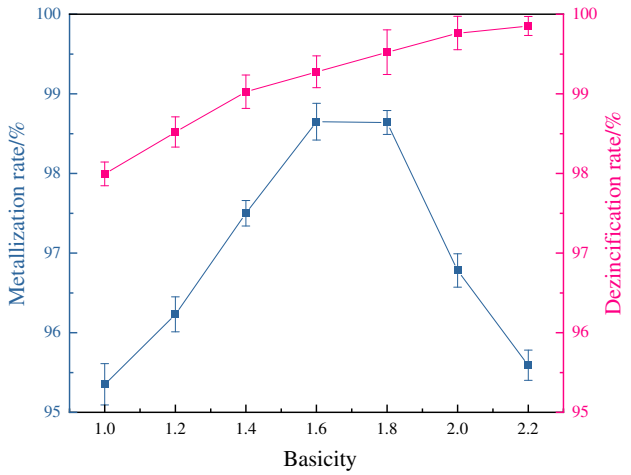

Fig. 7 Influence of R_4 on metallization rate and dezincification rate of metallized pellets

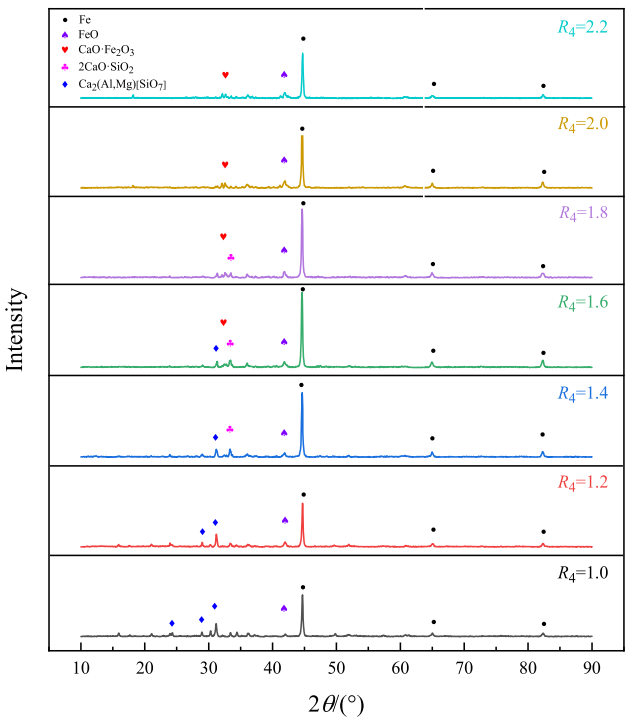

Fig. 8 Influence of R_4 on XRD patterns of metallized pellets

and iron oxides reduction were filled by silicates. The metallic iron was bonded, resulting in a dense internal structure of the pellets, contributing to the strength of the metallized pellets. The CaO and MgO act as network modifiers within the glass phase. The silicate network structure was disrupted due to the increase in basicity [47], and the proportion of silicate components in the liquid phase was reduced; thus, the compressive strength of the pellets was decreased. After the R_4 of the pellets is greater than 1.4, the proportion of calcium ferrite and calcium disilicate in the pellets is higher than that of the silicate phase. It can be noted that when the R_4 is between 1.4 and 1.8, the phase that plays the main bonding role in the pellets was $2CaO{\cdot}SiO_2$. The crystalline transformation of β-$2CaO{\cdot}SiO_2$ to γ-$2CaO{\cdot}SiO_2$ in the cooling process would lead to cracks in the pellets volume expansion [48]. The internal structure of the metallized pellets was destroyed, and thus, the strength of the pellets was further reduced. However, the generated voids facilitate the entry and release of reducing gases. The reduction of iron oxides to metallic iron was promoted, and the metallization rate and dezincification rate of the metallized pellets were increased. When the basicity was higher than 1.6, it can be clearly observed that the calcium ferrite phase gradually appeared and played a decisive role in the metallized pellets [49]. The amount of liquid phase further increased, and the strength of calcium ferrite was greater than that of the silicate phase; therefore, the compressive strength of the metallized particles was increased.

3.3 Effect of R_4 on microstructure of metallized pellets

To further explain the reason that R_4 affects the compressive strength of metallized pellets, the microstructure was analyzed using a Zeiss Axio Scope. A1 metallographic microscope. The phase composition ratios and void ratios were calculated semi-quantitatively based on the grayscale values of the different phases. Figure 9 displays the optical micrographs of typical pellet samples obtained from the seven experimental schemes. The contents of the major minerals and the void ratios were calculated and are presented in Fig. 10. It can be seen that the mineral composition of the metallized pellets mainly consists of a metallic iron phase (white), slag phase (blue) and voids (black). The formation of large voids inside the carbon-bearing pellets was caused by the combustion and volatilization of coke and organic binders, and the volume expansion resulting from the lattice transitions of the iron oxides reduced to metallic iron. This is one of the main reasons for the decrease in the strength of the pellets. The SiO_2 content was higher, forming low melting point silicates with Al_2O_3 and MgO when R_4 was lower. In this case, the slag phase and metallic iron phase are interwoven; thus, the void ratios can be effectively reduced. The contents of the metallic iron phase and slag phase decreased significantly when R_4 ranges from 1.4 to 1.8. The content of the metallic iron phase decreased from 33.97% to 24.12%, and the content of the slag phase gradually decreased from 30.56 to 6.44%. Also, the structure of the metallic iron phase transformed from flakes to dispersed iron grains. The number of voids increased from 35.47% to 69.45%, and the voids gradually transformed from small voids with uniform morphology to large irregular voids, causing a rapid decrease in the strength of the pellets. The reasons for this phenomenon can be known from the XRD results that the slag phase produced in this R_4 region was $2CaO{\cdot}SiO_2$. The crystalline transformation of β-$2CaO{\cdot}SiO_2$ to γ-$2CaO{\cdot}SiO_2$ leads to the appearance of cracks during the reaction process, destroying the internal structure and further reducing the strength of the metallized pellets. A large amount of CaO, SiO_2 and Al_2O_3 in high-basicity pellets enter the complex calcium ferrite when R_4 continues to increase. The calcium ferrite phase gradually increases, and the slag phase was increased from 6.44% to 13.57%. The calcium ferrite was distributed to form a mesh structure with metallic iron, replacing silicate as an important bonding phase in the pellets ore mineralization process. Moreover, the reduction reaction rate of pellets was improved by the relatively excellent reducing property of calcium ferrite. The calcium ferrite could promote the aggregation and connection of metallic iron crystals to form a larger area of the metallic iron phase. The metallic iron phase content was raised from 24.12% to 37.97%, thus inhibiting the reduction in malignant expansion of the pellets. The void ratios were reduced from 69.45% to 48.46%, which is a significant reason for the improvement in the strength of high-basicity pellets. The analytical results of mineral composition and void ratios of the pellets explained the effect of R_4 on the compressive strength of the metallized pellets.

3.4 Effect of R_4 on high-temperature properties of melt

Figure 11 shows the effect of R_4 on the high-temperature properties of the melt. The melt morphology at 800, 900, 1000, 1100 and 1200 °C and end-point temperature was given. The variation of melt area was analyzed by ImageJ software, and the curves of the effect of R_4 on the initial temperature of soft melting, soft melting speed and final soft melting area were obtained. The research performed by Zhao et al. [50] has shown that the reduction process of carbon-bearing pellets is divided into two stages: expansion period and contraction period. In the expansion period, the pellets are heated, and the reduction reaction of iron

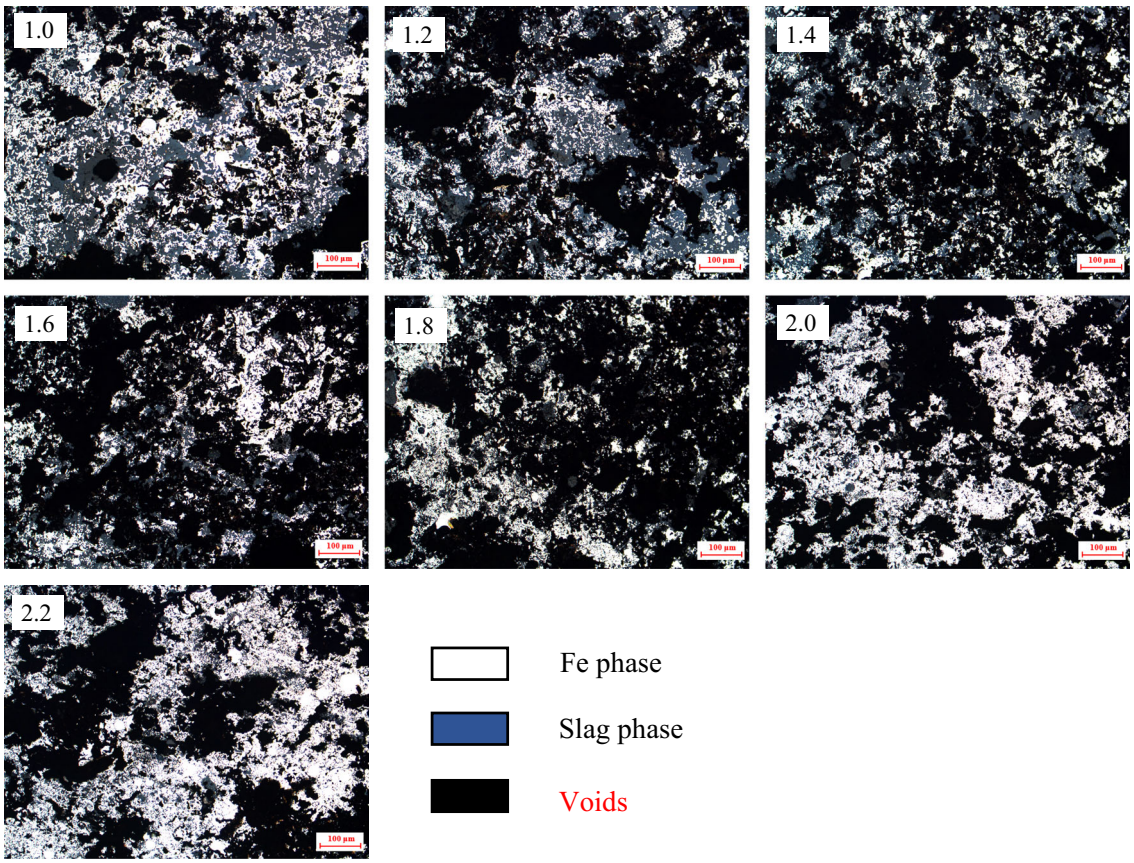

Fig. 9 Influence of R_4 on optical micrographs of metallized pellets

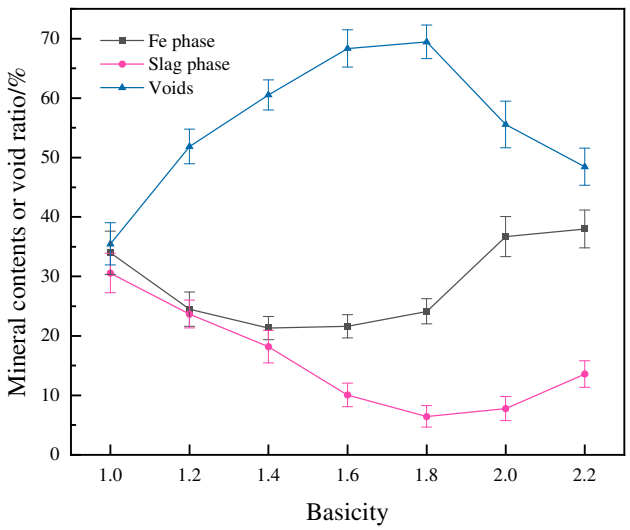

Fig. 10 Influence of R_4 on mineral content and void ratios of metallized pellets

oxide ($Fe_2O_3 \rightarrow Fe_3O_4$) begins to occur, resulting in the expansion of the pellets. In contraction period, the activity of iron oxide and carbon was increased with the rise in temperature, and the rate of reduction reaction was accelerated. The internal metal iron nuclei of the pellets were constantly formed, and fine metal iron crystals continuously migrate around the metal iron nuclei and gather to grow. Moreover, the slag phase was generated in large quantities, and the solid wastes particles were brought close to each other by the surface tension of the slag phase, so that the pellets shrink and densify. However, it can be clearly observed that the volume of the melt gradually decreases with the increase in temperature, without the phenomenon of expansion. The analysis suggests that, on the one hand, the iron oxide of the experimental material is mainly Fe_3O_4, which weakens the hazard of volume expansion brought by $Fe_2O_3 \rightarrow Fe_3O_4$. On the other hand, the voids are created inside the melt due to the different particle properties between mineral powder particles, and the heat volatilization of the carbon and organic binders, providing space for the volume expansion generated by the reduction of iron oxides in the specimens. This was consistent with the conclusions of the study of Wang et al. [51].

The final soft melting area of the melt showed a trend of first increasing and then decreasing with the increase in R_4. The maximum final soft melting area was 81% at R_4 of 1.8. The analysis shows that the liquid phase in this basicity range was mainly $2CaO{\cdot}SiO_2$ with a high melting point,

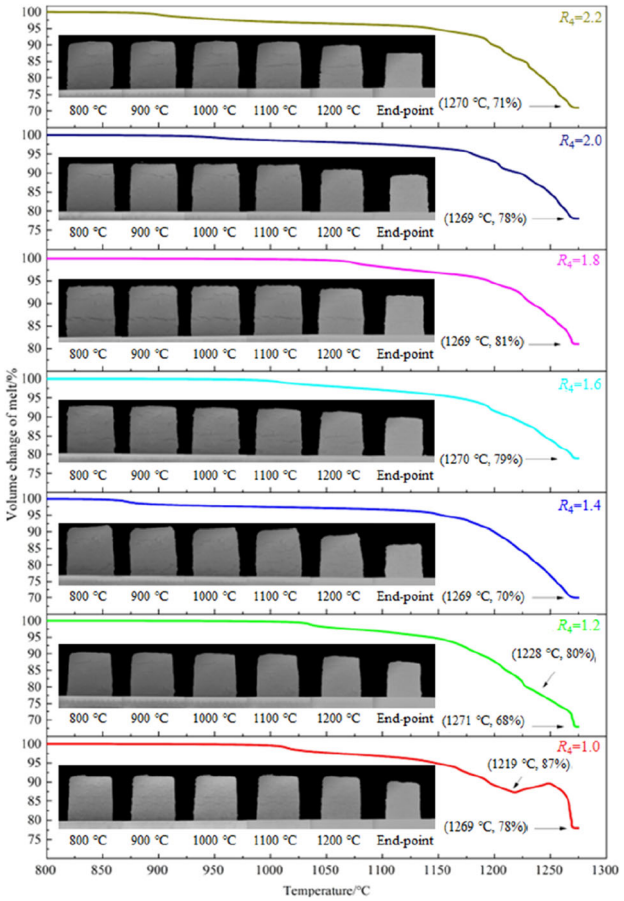

Fig. 11 Influence of R_4 on high-temperature properties of melt

causing a reduction in the production of the liquid phase in the reduced system and hindering the shrinkage of the pellets. However, when R_4 was lower ($R_4 < 1.4$) or higher ($R_4 > 1.8$), some low melting point compounds such as silicate and calcium ferrite are mainly generated in the system, thus causing the particles to shrink rapidly. In particular, when the R_4 was 1.0 and 1.2, the liquid phase was highly mobile due to the generation of excessive amount of liquid phase, hindering the contact between the iron oxide and the reducing agent. Meanwhile, a part of the liquid phase overflows with the reducing gas, resulting in the expansion of the pellets.

4 Conclusions

1. With the increase in R_4 from 0.6 to 2.2, the metallized pellets appeared in order with the phases of melilite, merwinite, bredigite and calcium disilicate. The content of the liquid phase in the generated slag phase showed a trend of first decreasing and then increasing. The content of FeO in the liquid phase remained stable with the increase in basicity, while the contents of SiO_2 and MgO decreased, and the contents of CaO and Al_2O_3 increased. Meanwhile, the increase in basicity leads to a decrease in the viscosity of the liquid phase from 1.55 Pa s (R_4 = 0.6) to 0.22 Pa s (R_4 = 2.2).
2. The compressive strength of metallized pellets shows a trend of first decreasing and then increasing with the increase in R_4. The minimum value was reached at R_4 of 1.6, and the compressive strength of metallized pellets was reduced from 2678.4 N/pellet (R_4 = 1.0) to 1521.9 N/pellet (R_4 = 1.6). A large amount of silicate makes the internal structure of the pellets become dense when R_4 was lower ($R_4 < 1.4$), which is an important reason for the increase in strength. It was a significant reason for the increase in the compressive strength of the metallized pellets. Notably, the compressive strength increases to 2099.6 N/pellet when R_4 continues to increase ($R_4 > 1.8$), due to the rise in the content of calcium ferrate which has better properties.
3. The area of the melt gradually decreases with the increase in roasting temperature, and no expansion phenomenon occurs. The final soft melting area of the melt showed a trend of first increasing and then decreasing with the increase in quaternary basicity, and the final soft melting area reached a maximum value of 81% at R_4 of 1.8. In particular, with the excessive amount of liquid phase generation at the lower R_4 ($R_4 < 1.4$), a part of the liquid phase overflows with the reducing gas, resulting in the expansion of the pellets.

Acknowledgements The authors are grateful acknowledges support from the Outstanding Youth Fund of Anhui Province (Grant No. 2208085J19) and the National Key Research and Development Program of China (Grant No. 2022YFC3901405).

Declarations

Conflict of interest We declare that there are no known conflicts of interest associated with this publication, and there has been no significant financial support for this work that could have influenced its outcome.

References

[1] L.K. Hong, J.J. Gao, Y.H. Qi, H.F. Wang, J. Iron Steel Res. 30 (2018) 703–709.
[2] C. Geng, H.J. Wang, W.T. Hu, L. Li, C.S. Shi, J. Iron Steel Res. Int. 24 (2017) 991–997.
[3] L.X. Qian, T. Yang, H.M. Long, L. Ding, C.C. Xu, ACS Sustainable Chem. Eng. 9 (2021) 16373–16383.
[4] J.S. Wang, Y. Li, H.X. Feng, Q.G. Xue, X.F. She, G. Wang, H.B. Zuo, Chin. J. Eng. 43 (2021) 1737–1749.
[5] L. Ding, Y.F. Wang, L.X. Qian, P.Y. Qi, X. Meng, H.M. Long, Fuel 338 (2023) 127268.

[6] W. Lv, M. Gan, X.H. Fan, Z.Y. Ji, X.L. Chen, J.W. Yao, T. Jiang, JOM 71 (2019) 3173–3180.
[7] Z. Chen, R.Q. Zheng, D.C. Ju, R. Mao, H. Ma, H.B. Peng, W.T. Du, J. Sustain. Metall. 8 (2022) 1001–1013.
[8] S. Kelebek, S. Yörük, B. Davis, Miner. Eng. 17 (2004) 285–291.
[9] Y. Li, H.X. Feng, J.S. Wang, X.F. She, G. Wang, H.B. Zuo, Q.G. Xue, J. Clean. Prod. 367 (2022) 132909.
[10] J.X. Zhang, C. Yang, F.S. Niu, S.L. Gao, J.J. Dong, Minerals 11 (2021) 1080.
[11] J.X. Zhang, W.G. Sun, F.S. Niu, L. Wang, Y.W. Zhao, M.M. Han, Int. J. Heat Technol. 36 (2018) 229–236.
[12] F.S. Niu, S.T. He, J.X. Zhang, C. Wen, Metals 12 (2022) 1856.
[13] Y.D. Xie, W.L. Xiong, J.X. Yu, J.Q. Tang, R.A. Chi, Process Saf. Environ. Prot. 116 (2018) 340–346.
[14] C. Sierra, J. Martínez, J.M. Menéndez-Aguado, E. Afif, J.R. Gallego, J. Hazard. Mater. 248–249 (2013) 194–201.
[15] N. Ma, J. Clean. Prod. 112 (2016) 4497–4504.
[16] A. Andersson, H. Ahmed, J. Rosenkranz, C. Samuelsson, B. Björkman, ISIJ Int. 57 (2017) 262–271.
[17] D.J.C. Stewart, A.R. Barron, Resour. Conserv. Recycl. 157 (2020) 104746.
[18] M.H. Morcali, O. Yucel, A. Aydin, B. Derin, J. Min. Metall. Sect. B 48 (2012) 173–184.
[19] D.Q. Zhu, D.Z. Wang, J. Pan, H.Y. Tian, Y.X. Xue, Powder Technol. 380 (2021) 273–281.
[20] D.Z. Wang, D.Q. Zhu, J. Pan, Z.Q. Guo, H.Y. Tian, Y.X. Xue, J. Iron Steel Res. Int. 29 (2022) 1559–1572.
[21] D.Z. Wang, D.Q. Zhu, J. Pan, Z.Q. Guo, C.C. Yang, X. Wang, T. Dong, JOM 74 (2022) 634–643.
[22] X.F. She, J.S. Wang, G. Wang, Q.G. Xue, X.X. Zhang, J. Iron Steel Res. Int. 21 (2014) 488–495.
[23] X. Xiao, S.F. Zhang, F. Sher, J.B. Chen, Y.T. Xin, Z.X. You, L.Y. Wen, M.L. Hu, G.B. Qiu, J. Sustain. Metall. 7 (2021) 340–357.
[24] I.F. Kurunov, Metallurgist 55 (2012) 634–639.
[25] B.P. Yur'ev, V.A. Dudko, Mater. Sci. Forum 1052 (2022) 467–472.
[26] R. Mao, F. Wang, H. Jin, S.D. Mao, Iron and Steel 55 (2020) No. 8, 199–205.
[27] C. Peng, J.F. Fan, Iron and Steel 54 (2019) No. 2, 97–100.
[28] E.H. Wu, R. Zhu, S.L. Yang, L. Ma, J. Li, J. Hou, J. Iron Steel Res. Int. 23 (2016) 655–660.
[29] R. Mao, L.Q. Ren, P. Du, F. Wang, J. Iron Steel Res. 29 (2017) 357–363.
[30] H.Y. He, H.L. Liu, Y.F. Cui, Y. Li, J. Ding, J. Iron Steel Res. 33 (2021) 196–201.
[31] W. Zhang, F. Wang, N. Li, ISIJ Int. 61 (2021) 1915–1926.
[32] S. Li, Z.S. Kang, W.C. Liu, Y.C. Lian, H.S. Yang, J. Sustain. Metall. 7 (2021) 126–135.
[33] S.F. Zhou, H.Y. Zheng, Y. Dong, X. Jiang, Q.J. Gao, M.F. Shen, Iron and Steel 56 (2021) No. 6, 15–20+27.
[34] W. Chen, X. Wang, Y. Lei, Y. Li, S.Q. He, Z.H. Liao, Iron and Steel 55 (2020) No. 9, 11–15.
[35] N. Li, F. Wang, L.M. Pan, J. Cent. South Univ. 29 (2022) 296–312.
[36] N. Li, F. Wang, W. Zhang, Metall. Res. Technol. 118 (2021) 209.
[37] R.F. Wei, J.X. Li, J.M. Li, H.M. Long, P. Wang, G. Gao, G.P. Lin, Chin. J. Process Eng. 11 (2011) 429–435.
[38] Y.G. Ding, J.S. Wang, X.F. She, G. Wang, Q.G. Xue, J. Iron Steel Res. Int. 20 (2013) 28–33.
[39] J. Ding, H.Y. He, Z.Y. Tang, Y. Li, H.L. Liu, J. Wuhan Univ. Sci. Technol. 44 (2021) 7–12.
[40] Y.S. Lee, D.W. Ri, S.H. Yi, I. Sohn, ISIJ Int. 52 (2012) 1454–1462.
[41] H.C. Chuang, W.S. Hwang, S.H. Liu, Mater. Trans. 50 (2009) 1448–1456.
[42] Q.M. Meng, J.X. Li, R.F. Wei, H.M. Long, T.J. Chun, P. Wang, Z.X. Di, L. Dessbesell, C.B. Xu, J. Iron Steel Res. Int. 25 (2018) 1105–1112.
[43] S. Mishra, G.G. Roy, Ironmak. Steelmak. 45 (2018) 426–433.
[44] D.C. Fan, W. Ni, A.Y. Yan, J.Y. Wang, W.H. Cui, J. Iron Steel Res. Int. 22 (2015) 686–693.
[45] E.H. Wu, J. Hou, J. Li, L. Ma, S.L. Yang, Iron and Steel 53 (2018) No. 1, 24–28.
[46] S. Zhang, W. Ren, J.L. Li, X.F. Zhang, Metall. Res. Technol. 114 (2017) 101.
[47] J. Li, H.F. An, W.X. Liu, A.M. Yang, M.S. Chu, J. Iron Steel Res. Int. 27 (2020) 239–247.
[48] H.Y. Yu, X.L. Pan, B.W. Liu, B. Wang, S.W. Bi, J. Iron Steel Res. Int. 21 (2014) 990–994.
[49] S. Ferreira, A. Cores, J.I. Robla, L.F. Verdeja, I. Ruiz-Bustinza, F. García-Carcedo, J. Mochon, Steel Res. Int. 85 (2014) 261–272.
[50] Y.X. Zhao, Z.X. Zhang, J.Y. Zhang, F.P. Yue, J.S. Wang, G. Wang, Sinter. Pelletiz. 42 (2017) No. 4, 19–22+53.
[51] G. Wang, Q.G. Xue, J.S. Wang, Thermochim. Acta 621 (2015) 90–98.